Monitoring Bodily Oscillation With RFID Tags

Youlin Zhang , *Member, IEEE*, Shigang Chen , *Fellow, IEEE*, You Zhou, *Member, IEEE*,
Yuguang Fang , *Fellow, IEEE*, and Chen Qian, *Member, IEEE*

Abstract—Traditional systems for monitoring and diagnosing patients' health conditions often require either dedicated medical devices or complicated system deployment, which incurs high cost. The networking research community has recently taken a different technical approach of building health-monitoring systems at relatively low cost based on wireless signals. However, the radio frequency signals carry various types of noise and have time-varying properties that often defy the existing methods in more demanding conditions with other body movements, which makes it difficult to model and analyze the signals mathematically. In this paper, we design a novel wireless system using commercial off-the-shelf RFID readers and tags to provide a general and effective means of measuring bodily oscillation rates, such as the hand tremor rate of a patient with Parkinson's disease. Our system includes a series of noise-removal steps, targeting at noise from different sources. More importantly, it introduces two sliding window-based methods to deal with time-varying signal properties from channel dynamics and irregular body movement. The proposed system can measure bodily oscillation rates of multiple persons simultaneously. Extensive experiments show that our system can produce accurate measurement results with errors less than 0.4 oscillations per second when it is applied to monitor hand tremor, even when the individuals are moving.

Index Terms—Radio frequency identification (RFID), sensor systems and applications.

I. INTRODUCTION

THE proliferation of radio frequency (RF) technologies has helped drive new healthcare products in recent years [1]–[7], as people become more and more health conscious, asking for better health and life-style management. The classical hospital-centered healthcare is shifting from diagnosis and treatment practice toward preventive care [8]–[11], with more and more people committing to disease prevention and early risk detection [12]–[14]. A key in preventive care is continuous monitoring, outside of clinics and in daily lives, which prefers nonintrusive and low-cost medical devices. Traditional health-monitoring systems require either dedicated medical

devices or complicated system deployment [12], [15], [16], which limits the locations of monitoring and incurs high cost. The networking research community recently takes a different approach of building health-monitoring systems based on wireless signals at relatively low cost [4], [7], [17], [18]. Adopting such an approach, this paper studies how to use RFID tags to accurately measure patients' hand tremor rates in a relaxed setting (e.g., at home) where patients can move around. Measuring the hand tremor rate helps monitor the conditions of a patient with Parkinson's disease (PD) [12], [19]. Together with the frequency and the pattern of occurrence, the rate measurement provides physical evidence for progression of the disease or for effectiveness of ongoing treatment with medicine, therapy or exercise routines. Continuous monitoring in daily lives is preferred, particularly because hand tremor happens intermittently. While we use hand tremor as an application example, our approach can also measure the oscillation rate of other body part, for example, by attaching a tag to the chest of a patient's shirt for respiration rate measurement.

RF-based technologies for monitoring human activities [2]–[7] have drawn much attention from the research community recently, thanks to their low cost and easy deployment. For example, Adib *et al.* [2] leveraged frequency modulated continuous wave (FMCW) radar and universal software radio peripheral to detect the oscillation of human chest caused by respiration, through which they obtain the breathing rate of that person. However, this system is not feasible in practice since it is hard to deploy and requires specialized devices of high complexity. Patwari *et al.* [3] extracted the coarse-grained received signal strength (RSS) from the wireless sensor nodes to estimate the human respiration rate. This approach requires deployment of multiple (more than 12) dedicated sensor nodes, which is cumbersome and resource costly. UbiBreathe [6] estimates the human respiration rate by measuring the RSS of WiFi signals. It can produce more accurate measurement results than the above sensor-based system. However, it requires a user to lay down and place a mobile device on the chest, which is much inconvenient; otherwise, if the device is placed by the side of the person, the accuracy of the measurement results significantly degrades. The system designed by Liu *et al.* [4] provided a device-free solution for tracking vital signs during sleep. It extracts the fine-grained channel state information (CSI) [20] using WiFi devices to track the breathing rate and the heart-beat rate of a person in bed. Again, the person has to stay still in order to avoid introducing disturbance to WiFi signals. Therefore, the system cannot support continuous monitoring in day time when the person may move around,

which is a condition assumed in this paper for hand tremor monitoring as hand tremor can come and go and may happen at any time. Another limitation is that it can simultaneously monitor two persons at most. The designs of the above systems are mostly geared toward measuring respiration rates under static, restrained settings, not for tremor rates, which are much faster at multiple ticks per second and are measured under dynamic settings allowing free movement.

Also related is Tagbeat [21], which is designed to measure the high-frequency vibration induced by machines (e.g., engine and centrifuge) or the fundamental frequency of physical objects (e.g., buildings). Its method based on compressive sensing assumes that the vibration signals can be mathematically modeled as near-perfect periodic curves with a small number of stable parameters in the spectrum domain. This assumption does not hold for human-body oscillations which, unlike machines, carry significant irregularity both in oscillations themselves (such as hand tremor) and in other bodily itself have many time-varying wireless properties from both channel dynamics and irregular body movement. Our experiments will clearly show that the resulting signal curves cannot be modeled as perfect periodic curves for the methods in [21] to apply. Additional related work on wearable sensors [17], [22], [23], electromyography (EMG) [16], and polysomnography (PSG) [15] will be discussed shortly.

To address the limitation of the prior systems, we propose and build an RFID-based easily deployable wireless system for measuring hand tremor rate (or other bodily oscillation rate) in dynamic settings where wireless signals are not perfectly periodic. RFID technologies have gained popularity in recent years. Numerous applications have been developed, including inventory control, supply chain management, product tracking, and indoor localization [18], [24]–[32]. A typical RFID system consists of a reader and many tags, forming a simple reader-tag wireless network. Tags are very cheap and convenient to deploy, which helps promote their widespread use. With this advantage, the proposed system is unique with its capability of accurately measuring hand tremor rates of multiple persons, even when they are moving around. While this paper focuses on hand tremor rate, we will show experimentally that our system can be used to measure other bodily oscillation rate as well by attaching an RFID tag to body part under measurement or the immediate clothing to that body part. Because an RFID reader can easily distinguish the backscatter signals from multiple tags, our system is able of simultaneously measuring the oscillation rates of different tags attached to multiple persons or different places on the same person. Using only commercial off-the-shelf RFID readers/tags, the system is designed to work in either hospital/clinic settings where multiple patients can be monitored simultaneously or home settings where patients may borrow mobile readers from hospitals to perform continuous monitoring with the comfort at home. Tags cost as little as a dime a piece. They can be tossed away after being used, which is desirable in medical context.

Our system measures the phase values of RF signals in tag-reader communication and estimates oscillation rate based on the periods in phase change. An RFID reader can measure two important properties of the RF signals: RSS values and phase values. The RSS values of weak RFID signals do not work well for our purpose due to the following reasons: on the one hand, oscillation on human body is a small movement, which produces very small changes in RSS. On the other hand, the measurement of RSS by a commercial reader is noisy and coarse, with a resolution of 0.5 dB [33], so that the small bodily movement will not even affect the reported RSS values. In contrast, the phase resolution by a commercial reader is high, reaching 0.0015 rad [33], which translates to a spatial resolution of 0.04 centimeters. Such a fine spatial resolution enables us to catch slight oscillations such as hand tremor.

There are several technical challenges in the design of our system. First, the phase values measured by a reader are not well-shaped due to environmental noise, device imperfection, and measurement errors. Second and more importantly, unlike machine-produced vibrations, human's bodily oscillation is time-variant. The irregularity in oscillation makes it difficult to model precisely or analyze mathematically. Third, for hand tremor that can come and go and may happen at any time, it is helpful to support monitoring over a longer period of time in a relaxed setting where patients can move around. However, such moving introduces unpredictable changes in the measured phase values. We develop a series of methods to handle the above challenges by removing noises from various sources and by introducing two sliding window-based methods to process time-varying phase data, from which we reveal the oscillation pattern and derive the oscillation rate accurately.

We have built a prototype system for performance evaluation, which shows that the proposed system can accurately estimate hand tremor rate under a variety of settings: when measuring the hand tremor rate of a single person who sits, the average error is 0.11 tick per second (tps); when simultaneously measuring the hand tremor rates of four persons who sit, the average error is just 0.14 tps; when simultaneously measuring the hand tremor rates of four moving persons, the average error is 0.26 tps.

The rest of this paper is organized as follows. Section II provides a review of related work. Section III presents the architecture and an overview of our system. The technical details are elaborated in Section IV and the experiment setup is described in Section V. In Section VI, we evaluate the performance of our system and discuss the experimental results. Finally, we discuss some limitations of our system in Section VII and conclude this paper in Section VIII.

II. RELATED WORK

Research in patient activity monitoring can be classified into three categories: 1) dedicated sensor-based; 2) smart phone and wearable device-based; and 3) RF signal-based.

Traditional methods for activity monitoring use dedicated sensors. For example, Patel *et al.* [12] leveraged wearable sensors to monitor PD with the collected data relayed to a remote clinical site via a Web-based application. Albani *et al.* [16] used EMG to study tremor in PD, detect basic body postures, and study gait in PD patients. PSG [15] attaches multiple sensors to a patient to monitor human health conditions including respiration rate, heart beat rate, eye movements,

and muscle activity. This kind of technique requires specialized devices, which can make people uncomfortable in use. Besides, additional network infrastructure is needed for collecting and processing the data.

Recent research exploits embedded functions of smart phones and wearable devices such as accelerometers and GPS to monitor patient activities [17], [22], [23]. For example, Hao *et al.* [17] used the microphone of a smart phone to measure sleep quality, with detection of sleep events such as body movement, couch, and snore. But it cannot quantitatively measure the bodily oscillation rate of human bodies such as hand tremor rate. PERFORM [23] proposes an intelligent close-loop system which integrates four wearable sensors to monitor activities of the PD patients. These sensors are more costly and less comfortable to wear than RFID tags, which are small, thin, flexible, and easily attachable to body or cloth.

Most related to this paper is the RF signal-based approach for human activity monitoring. Some systems use Doppler radars [34], ultrawideband (UWB) radars [35], [36], or FMCWs radars [5]; others rely on measurement of RSS [3], [6], CSI [4], [7], or phase values [18], [21]. Specifically, the systems [3], [5], [35], [36] that require specialized devices such as Doppler radars, UWB radars, or wireless sensors incur high cost, and they require trained personnel to deploy. While UbiBreathe [6] improves accuracy over [3] in estimating respiration rate based on RSS measurements, it achieves its best accuracy with an error smaller than 1 breath per minute (b/min) when it places a mobile device on a patient's chest. Under the device-free mode, it has an error greater than 1.5 b/min, and this mode imposes that the patient being monitored has to stay in the line-of-sight (LOS) between a wireless transmitter and a receiver. Liu *et al.* [4] proposed a system utilizing fine-grained CSI for measuring a patient's breathing rate and heart rate. Their method is device-free but relies on relative positions of the patient and WiFi devices used. In addition, the system cannot be applied to more than two persons simultaneously. Wang *et al.* [7] proposed another WiFi-based breathe monitoring system that improves over [4], [6]. This system uses WiFi Fresnel zone to monitor human respiration. It can accurately measure human respiration rate under arbitrary body orientation and posture. It also can only monitor two persons at once. TagBreathe [18] uses the phase values of RFID tags to monitor respiration rate and can support multiple users. Like [4] and [7], it does not consider dynamic settings that allow patients to move around for continuously monitoring in daily life activities. The design of the above systems heavily relies on positioning of devices and patients. Also related is Tagbeat [21], which measures the rotation period of a centrifuge machine. Its method is applicable to measuring wind speed, monitoring centrifugation, and troubleshooting engine [21]. It requires static and steady conditions where the mechanical vibration of an object produces near-perfect periodic cures in wireless signals, which are time-invariant in the spectrum domain. This is a condition that does not hold for oscillations in human body such as hand tremor that carries inherent irregularity in both frequency and magnitude.
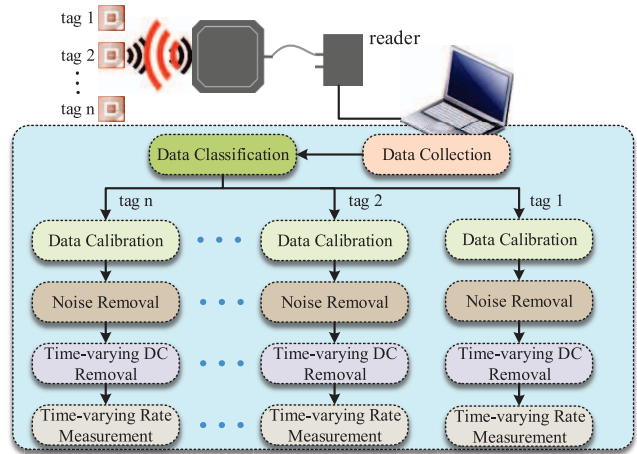

Fig. 1.   Our system architecture.

III. SYSTEM OVERVIEW

The goal of our system is to measure the bodily oscillation rate, using hand tremor as a study case. The system deployment is simple: an RFID tag is attached to the hand (or other body part) under monitoring. An RFID reader is deployed in the room to continuously measure the phase values of the wireless signals backscattered from the tag. The patient is allowed to move within the coverage area of the reader. Multiple tagged patients can be monitored simultaneously.

The basic idea behind our approach is that when a hand attached with an RFID tag shakes, this oscillation will introduce a periodic component in the reported phase values. Therefore, we can analyze the collected phase values and extract this periodic pattern. Once the oscillation pattern is captured, the hand tremor rate can be estimated. The challenge is that bodily oscillations have many time-varying properties, which make it much more difficult to handle than the machine-produced near perfect oscillations that can be precisely modeled mathematically. We introduce two sliding window-based approaches to deal with the time-varying properties. The accuracy of our system is confirmed through experimental studies. Moreover, since RFID tags will report their unique IDs, we can easily differentiate the phase values of one person from those of others using the reported tag IDs. Thus, the solution for estimating the hand tremor rate of a single human can be extended to the multiperson case.

Our system in Fig. 1 consists of six modules: 1) data collection; 2) data classification; 3) data calibration; 4) noise removal; 5) time-varying direct current (dc) removal; and 6) time-varying rate measurement. All these modules can be implemented on a laptop connected to an RFID reader. Assume we have n people to be monitored, each of which is attached with a tag on his hand (or chest). Our system first collects the phase values of the tags by an RFID reader. The collected data is then processed by the data classification module, which classifies the data into different groups based on the reported tag IDs. After data classification, the data of each group will be processed separately by the data calibration module, the noise removal module, the time-varying dc removal module, and the time-varying rate measurement module, which
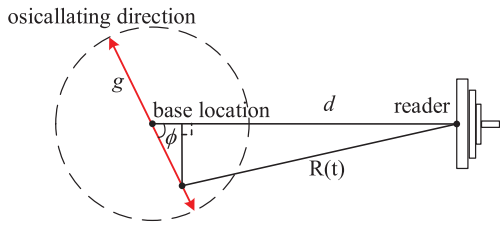
Fig. 2. Hand tremor model.

outputs the oscillation rate. The details of these modules will be elaborated in Section IV.

IV. System Design

In this section, we present the functional details of our system on how the phase values are processed step by step to produce an estimated oscillation rate. While we will discuss the measurement of respiration rate at the end of this section, most of our presentation concentrates on measuring the hand tremor rate of any person based on the set of phase samples from the tag of that person. In the sequel, we use the terms, "tremor" and "tremble," exclusively for hands, and the terms, "static," "moving," and "movement," for other larger bodily movement such as moving an arm or walking. For example, when we say "hand tremor rate of one *static* person," the word static means that the person does not have any other bodily movement except that one of his hands trembles. With "hand tremor rate of one *moving* person," we mean that the person may be waving his arm or walking when one of his hands trembles. For the cases of measuring hand tremor rates of multiple persons, we allow the individuals to move as they wish.

A. Time-Varying Properties

Before we elaborate the design of our system, we first mathematically analyze the time-varying properties of a tag's phase values when it is attached to a trembling hand. We begin by examining the ideal motion in [18] where a tag oscillates in perfect harmonic motion along the direction of the double arrow in Fig. 2. The middle point of the double arrow is called the base location of oscillation. Let d be the distance between the base location and the reader's antenna, ϕ the acute angle between the line of oscillation and the line from the reader to the base location, r the rate of oscillation, and g the magnitude of oscillation.

Consider harmonic motion in which the distance from the tag to the base location can be modeled as $g \sin(2\pi rt)$. From the figure, it is easy to see that the tag-reader distance $R(t)$ is

$$R(t) = \sqrt{(d - g\sin(2\pi rt)\cos\phi)^2 + (g\sin(2\pi rt)\sin\phi)^2} \tag{1}$$

which has a period of $(1/r)$. As the tag-reader distance changes over time, it creates a phase shift in the backscattered signal received by the reader. Today's reader can typically produce around 40 phase samples per second at random times based on an arbitration protocol that resolves collision when multiple tags are present [37]. Each sample includes the tag ID, the time

when the sample is taken, and the phase. For an oscillation characterized by (1), the phase $\theta(t)$ can be modeled as

$$\theta(t) = \theta_0 + 2\pi \frac{2R(t)}{\lambda} \qquad \mod 2\pi \tag{2}$$

where an offset θ_0 is introduced by the hardware, λ is the wavelength of the RF waves, and the total distance traveled by the waves from the reader to the tag and back to the reader is $2R(t)$.

Clearly, $\theta(t)$ is a periodic curve, with a period of $(1/r)$. It has been shown in [21] that a periodic phase curve can be approximately recovered from discrete random samples (produced by the reader) using the method of compressive sensing. The assumption is that the curve has nearly perfect periods where the phase repeats the same values in each period, as is the case of machine-induced vibrations studied in [21] and also is the case in the ideal model of (1) and (2) above.

However, this paper studies the oscillations produced by human body, which have time-varying properties that break the above assumption. For example, consider that a tagged hand trembles. The oscillation rate r may change over time. The tremor magnitude g may also change over time. The person may walk around, and therefore d and ϕ change over time. In this situation, $\theta(t)$ is no longer a periodic curve in the mathematical sense. It can be a complex, nonrepeating curve that shows oscillation but defies the use of compressive sensing and other methods that assume mathematically periodic curves. To reflect the time-varying properties, the model of (1) and (2) has to be rewritten as

$$R(t) = \sqrt{\begin{aligned}&(d(t) - g(t)\sin(2\pi r(t)t)\cos\phi(t))^2 \\ &+ (g(t)\sin(2\pi r(t)t)\sin\phi(t))^2\end{aligned}}$$
$$\theta(t) = \theta_0 + 2\pi \frac{2R(t)}{\lambda} + \varepsilon \qquad \mod 2\pi \tag{3}$$

where ε is an error caused by environmental noise. Such a model is hard to analyze using the traditional methods. Therefore, new ways must be invented to find the oscillation rate not based on model analysis but-based directly on the time-varying phase samples. Before explaining the details of our approaches, we first describe how we collect data from users.

B. Data Collection and Classification

Suppose we have n users, each of which is attached with an RFID tag to a finger and each tag has a unique ID. The reader continuously interrogates the tags, which respond by backscattering the RF signals from the reader. The reader performs a collision-resolving arbitration protocol [37] that allows it to communicate with the tags in turn, collecting the individual tag IDs and the associated physical-layer signal properties such as phase shift and RSS.

Fig. 3 shows an example of the collected phase values from four moving people when their hands (tags) are trembling. In this figure, each point represents a phase sample we have collected. Since the four tags' phase values are randomly sampled and mixed together in the data, we cannot observe any periodic pattern. Fortunately, the phase samples are collected
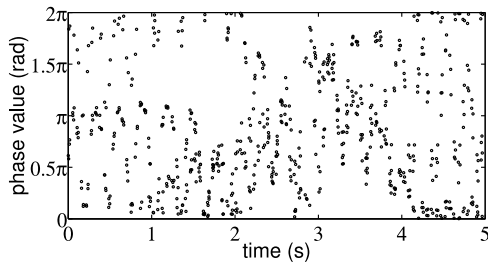
Fig. 3. Phase samples when four people move with their hands trembling.

Fig. 5. Phase values from a single static person after spikes are removed.
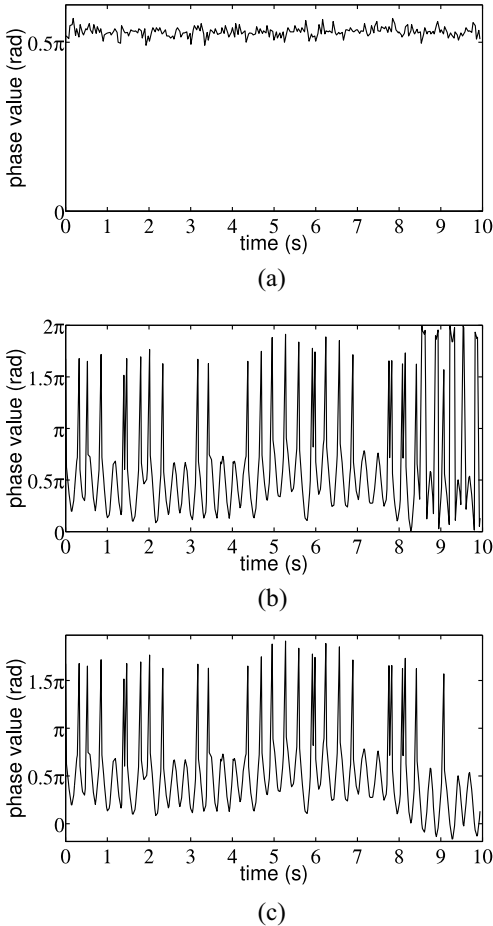

(a)

(b)

(c)

Fig. 4. Phase samples produced by a reader for a tagged person. Phase samples when (a) a person stays still without hand tremor and (b) a person has one hand trembling. (c) Phase samples after data calibration.

together with tag IDs, which allows us to easily separate the data into four groups, one for each tag. We can then process each group of data at a time to obtain the hand tremor rate of one person. In the following, we will focus on the data from one person.

C. Data Calibration and Noise Removal

Consider the set of phase samples produced by an RFID reader for a specific tag. These samples are inherently noisy due to environment interference and product properties [33]. Fig. 4(a) shows the phase samples recorded by the reader from one tagged person whose hand stays still; refer to Section V for details of the testbed. Note that we connect the adjacent phase
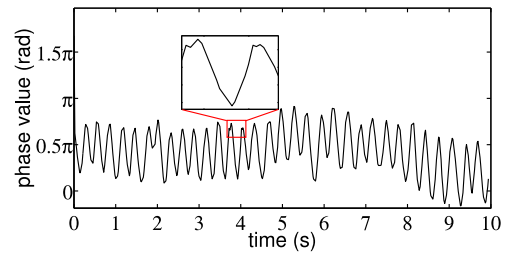
values in the figure to show a phase curve with spikes whose tips are where the phase samples locate. The phase curve stays largely a constant with small random noise fluctuations.

Fig. 4(b) shows the phase samples when the person emulates hand tremor by shaking one hand while sitting by a desk without other bodily movement. The curve in the figure is noisy. The time-varying noise is caused by various factors, including device properties and fluctuations in the distance between the reader and the base location of the tag, in the oscillation rate, and in the oscillation magnitude. Simply applying a low pass filter will not work well. Although it can remove high-frequency noise (such as white noise from the environment), as we will show, much of the noise in our measurement is not of high frequency, which makes the low pass filter ineffective.

Our first observation is that, when the tag moves to a location where the true phase value is close to a multiple of 2π's, as the noise pushes it back and forth around this multiple, the modulo operation in (2) may cause 2π jumps up or down in the reported phase samples.

Such large errors are evident in Fig. 4(b) between 8 and 10 s. To calibrate the phase samples, we enforce continuity in phase changes. If there is a sudden change of about 2π between two consecutive phase values, we know that it is caused by the modulo operation. In this case, we need to remove the sudden 2π change to ensure the continuity between the two phase values. After data calibration, the phase curve becomes Fig. 4(c).

Second, not all noise in the phase curve is caused by modulo operation. Tags are very cheap hardware, and there is device imperfection [33], with isolated π shift in some reported phase values, as we have observed in our experiments using different tags. For example, in Fig. 4(c), as the basic shape of the phase curve fluctuates between 0 and π, there are spikes of magnitude π into the range of $[\pi, 2\pi)$. In this experiment, the operating frequency is 920 MHz, which means a wavelength of about 32.6 cm. The sampling rate for phase values is around 40 samples per second. The magnitude of hand tremor is smaller than half of a wavelength, which means it is not possible for two consecutive phase-value samples to be apart by π. Therefore, as another noise removal operation, whenever we see a phase jump of more than π between two consecutive phase values, we will reduce the second value by π. After noise removal, the phase curve becomes Fig. 5.

Third, after removing the noise caused by modulo operation and device imperfection, we observe that there is still undesired noise in the data. The remaining noise comes from the

environmental interference and can degrade the performance of our method for measuring the oscillation rate based on the number of peaks (or valleys) in the phase curve. As we zoom-in to see the details in Fig. 5, there are some small unexpected peaks (called *false peaks*) in the curve that will interfere with our measurement.

Thus, we adapt a wavelet based denoising algorithm [38] in our context to remove noise in the phase curve. Traditional methods that use a low (or band) pass filter with cut-off frequency cannot effectively deal with this problem, because the noise may be in the band of the signals, for example, when it is created due to the tagged person's other movement (such as waving arms).

The wavelet transform was originally introduced to overcome the limitation of Fourier transform for time-frequency analysis of signals. We decompose the oscillation phase $\theta(t)$ using discrete wavelet transform (DWT) as

$$\theta(t) = \sum_k A(l_0, k)\phi_{l_0,k}(t) + \sum_{l=l_0}\sum_k D(l, k)\psi_{l,k}(t) \quad (4)$$

where l_0 is the initial resolution, $\phi_{l_0,k}(t)$ is the discrete scaling function, and $\psi_{l,k}(t)$ is the discrete wavelet function, with the two functions orthogonal to each other. $A(l_0, k)$ and $D(l, k)$ are the approximation and detail coefficients at each level, which are filtered in the denoising process. These coefficients are defined as

$$A(l, k) = \langle \theta(t), \phi_{l,k}(t) \rangle$$
$$= 2^{-l/2} \int_{+\infty}^{-\infty} \theta(t)\phi_{l,k}\left(2^{-l}t - k\right)dt \quad (5)$$
$$D(l, k) = \langle \theta(t), \psi_{l,k}(t) \rangle$$
$$= 2^{-l/2} \int_{+\infty}^{-\infty} \theta(t)\psi_{l,k}\left(2^{-l}t - k\right)dt. \quad (6)$$

After decomposing the phase curve, we set a threshold λ_M for the noise level and remove the noisy coefficients from the original curve $\theta(t)$. In this paper, we choose the minimax threshold algorithm [39] for threshold selection. The minimax threshold algorithm is an optimization problem in which an optimal threshold is selected to minimize the maximum mean square error and obtain the worst risk function against an ideal process. The optimal threshold we want is defined as

$$\lambda_M = \sigma \lambda_n^* \quad (7)$$

where λ_n^* refers to the value of λ, which is obtained by optimizing the object function as follows:

$$\Lambda_n^* := \inf_\lambda \sup_d \frac{R_\lambda(d)}{n^{-1} + R_{\text{ideal}}(d)} \quad (8)$$

where d is one of the total n coefficients we obtain through DWT and the risk is calculated as $R_\lambda(d) = E(\delta_\lambda(d) - d)^2$. R_{ideal} is the ideal risk, which states whether or not to keep an empirical wavelet coefficient and is given by

$$R_{\text{ideal}}(d) := \min\left(d^2, 1\right). \quad (9)$$

Finally, we choose the approximation and detail coefficients based on the threshold λ_M and use them to reconstruct the signal without noise. We denote the set of phase samples after the above noise removal as Θ^*.
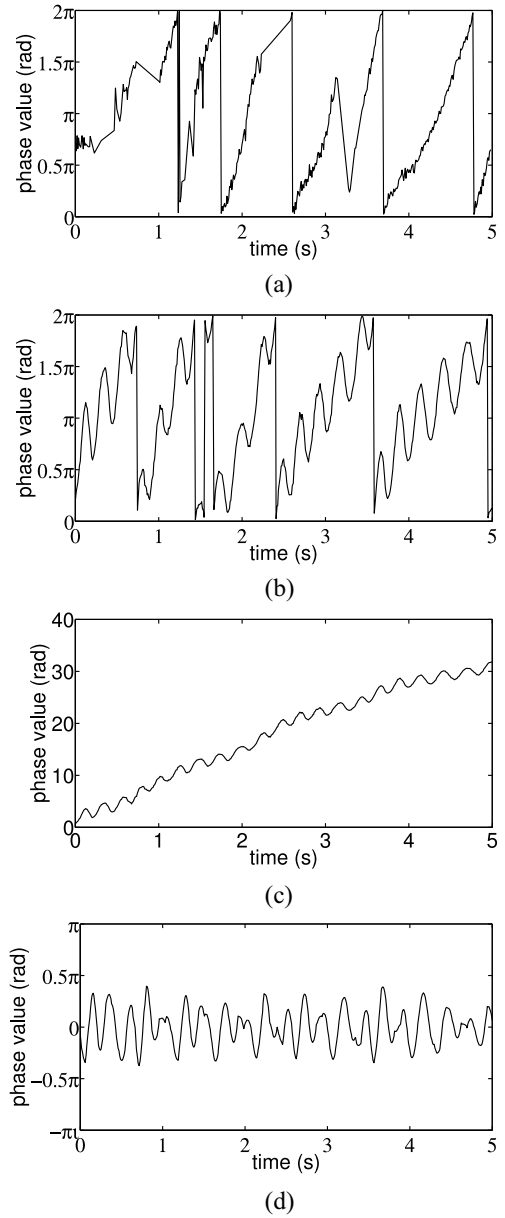

Fig. 6. Sliding window-based approach for removal of time-varying dc. Phase samples when (a) a person moves without hand tremor and (b) a person moves with one hand trembling. Phase samples after (c) noise is removed and (d) time-varying dc is removed.

D. Time-Varying DC Removal

There exists a time-varying dc component in the curve, which is partially resulted from the instability of hand when it trembles: suppose trembling is a cyclic motion around the base location of a hand. Even for a static person without large bodily movement of walking or arm waving, the base location of the hand may still shift slightly over time. If the person actually moves around, the time-varying dc component will be more significant. Fig. 6(a) shows the phase samples measured in an experiment where a person walks at a speed around 0.3 m/s with a tag attached to his hand. As the person moves without his hand trembling, the phase value changes steadily, in addition to small high-frequency fluctuations due to environmental noise. When the curve reaches 2π, it will drop to zero

due to the modulo operation. Fig. 6(b) shows the phase samples taken when the person walks at a speed around 0.3 m/s, with his hand trembling. The phase shift is caused by a combination of hand tremor and the person's moving. In addition, at the boundary of 2π or zero, instability in phase measurement due to hand tremor may cause 2π swings in the module operation, which is evident between 1.5 and 2 s in the plot. Fig. 6(c) shows the phase values after data calibration (spike removal) and noise removal. Comparing this plot with Fig. 4(b), we can see that a person's movement introduces a much greater, time-varying dc component in the phase curve. More significantly, alongside the dc component, there are false peaks (between 2 and 4 s) that are not eliminated by the noise removal module, possibly because this noise's frequency is too close to the rate under measurement. Fortunately, we find that by removing the time-vary dc component, we can also remove this noise.

We model the phase sample $\theta(t) \in \Theta^*$ after noise removal as

$$\theta(t) = a + M(t) + \hat{\theta}(t) \tag{10}$$

where a is a constant dc component which is dependent on the initial distance between the tag and the reader's antenna, as well as hardware properties, $M(t)$ is a time-varying dc component due to the shift of the hand's base location, and $\hat{\theta}(t)$ is the oscillating component caused by the hand trembling around the base location. We want to approximately remove $a + M(t)$ from the samples $\theta(t)$ to find the values of $\hat{\theta}(t)$. If trembling is steady as a harmonic motion, $\hat{\theta}(t)$ can be modeled by (3). But in real life, a hand may tremble with time-varying magnitude and rate.

A naive approach of removing dc is to subtract $\theta(t)$ by the global mean of the phase samples. However, this approach does not work well since it will only transpose the phase curve along the vertical axis. We propose a sliding window-based approach that computes a local mean within a sliding window for dc removal. The local mean $l(t)$ at time t within window $[t - (W/2), t + (W/2))$ is defined as

$$l(t) = \frac{1}{W} \int_{t-\frac{W}{2}}^{t+\frac{W}{2}} \theta(t')dt'$$

$$= \frac{1}{W} \int_{t-\frac{W}{2}}^{t+\frac{W}{2}} \left[a + M(t') + \hat{\theta}(t') \right] dt' \tag{11}$$

where W is the size of the window. Within a small time window, we assume $M(t')$ is approximately a linear function and $\theta(t')$ is approximately a periodic function. For example, consider a patient walks around indoor with a hand trembling. Within a time frame of a few seconds, the patient is *likely* to be moving along a line. Even though the patient will make turns, as long as the assumption is roughly satisfied for most such time windows, our approach will work well overall. With the above approximations, we have

$$l(t) \approx a + M(t) + \frac{1}{W} \int_{t-\frac{W}{2}}^{t+\frac{W}{2}} \hat{\theta}(t')dt'. \tag{12}$$

Note that $M(t)$ is the mean of $M(t')$ in the window $t' \in [t - (W/2), t + (W/2))$. By definition, $\hat{\theta}(t')$ is the oscillating curve after the dc component is removed. Hence, its integral over each period is zero. When W is much larger than the period length, the value of $(1/W) \int_{t-(W/2)}^{t+(W/2)} \hat{\theta}(t')dt'$ becomes insignificant when comparing with the magnitude of the $\hat{\theta}(t')$ curve. Hence, we have

$$l(t) \approx a + M(t) \tag{13}$$

which is exactly what we want to remove as the time-varying dc component. We can approximately compute the value of $l(t)$—thus the value of $a + M(t)$—from (11) based on the phase samples taken in the time window $[t - (W/2), t + (W/2))$. Let $S(t) \subset \Theta^*$ be the subset of phase samples in this window. For each sample $\theta(t')$ taken at a specific time t', let $\Delta(t')$ be the time interval from this sample to the next sample. We approximate the integral in (11) with discrete samples as follows:

$$l(t) = \frac{1}{W} \sum_{\theta(t') \in S(t)} \theta(t') \times \Delta(t') \tag{14}$$

where $S(t)$ and $\Delta(t')$, $\forall \theta(t') \in S(t)$, can be easily found from the full set Θ^* of phase samples.

The exact value of W should be determined based on the application context. It should be small enough such that $M(t)$ is likely to be linear within a time window, and it should be significantly larger than the oscillation period. To measure the hand trembling rate of a patient indoor, a few seconds should be appropriate. After the local mean $l(t)$ is computed, we subtract it from $\theta(t)$ as follows:

$$\hat{\theta}(t) = \theta(t) - l(t) \qquad \forall \theta(t) \in \Theta^*. \tag{15}$$

The set of resulting phase values is denoted as $\hat{\Theta}$. For mathematical rigor, we point out that additional phase samples should be taken during a period of $[(\max\{W, \hat{W}\})/2]$ preceding the first sample in Θ^* and a period of the same length after the last sample in Θ^*, where $\hat{W}$ is the width of another sliding window introduced later.

By applying a sliding window step by step over the whole curve, we are able to remove the time-varying dc, as shown in Fig. 6(d), which characterizes the phase shift due to hand tremor alone.

E. Time-Varying Oscillation Rate

Unlike a machine that can produce a perfectly periodic phase curve, the oscillation from a human body (such as hand tremor) may be time-varying. Not only may the magnitude be time-varying, but the oscillation rate (or equivalently the tremor period) can also change over time. Moreover, the phase curve produced by connecting the samples in $\hat{\Theta}$ is a distorted representation of the oscillation movement. The shape of the curve is dependent on the time instances when the phase samples are taken, which are random according to the operation of an RFID reader.

To compute time-varying oscillation rate, we again resort to a sliding window-based approach. We compute the oscillation rate $r(t)$ at time t from the phase samples in the time window $[t - (\hat{W}/2), t + (\hat{W}/2))$, where $\hat{W}$ is the window size, which is application-dependent. For example, when measuring hand

tremor, a period of a few seconds should be appropriate as the rate is likely to remain similar in such a short period of time. We first identify the peaks (or valleys) within the window on the phase curve. We then use the peak-to-peak distances to estimate the tremor period and compute the oscillation rate.

Let $\hat{S}(t)$ be the subset of phase samples from $\hat{\Theta}$ in the window of $[t - (\hat{W}/2), t + (\hat{W}/2))$. A simple algorithm for identifying peaks is to compare each phase sample in $\hat{S}(t)$ with its preceding sample and its successive sample.[1] If the phase sample is greater than both its predecessor and successor, we treat it as a peak. In Section IV-C, we use the DWT method to remove the false peaks caused by the environmental noise. It can indeed remove the majority, but not all, of the false peaks, as we observe in our experiments. Below we will temporarily leave this problem and come back to address it shortly.

After we identify all the peaks on the window, we obtain an estimation $p(t)$ of the tremor period using the least-squares method. We denote the peak-to-peak intervals as $\{v_1, v_2, \ldots, v_i, \ldots, v_m\}$. The least-squares estimation is given as

$$\arg \min_{p(t)} \sum_{i=1}^{m} (p(t) - v_i)^2. \tag{16}$$

The oscillation rate $r(t)$ at time t, as estimated within the window of $[t - (\hat{W}/2), t + (\hat{W}/2))$, is

$$r(t) = \frac{1}{p(t)}. \tag{17}$$

We now go back to address the problem of remaining false peaks. Our observation is that the interpeak interval is expected to be around p. If two peaks are too close to each other and their interpeak interval is below a threshold, e.g., half of $p(t)$ in our experiments, we remove the peak with smaller magnitude of the two. If two peaks are too far away from each other and their interpeak interval is above a threshold, e.g., twice of $p(t)$ in our experiments, we add another peak in the middle with the average magnitude of the two. After all such peak removal and addition, we compute (16) again for a new estimation of $p(t)$ and a new oscillation rate $r(t)$. The above process repeats until there is no further peak removal or addition.

The average oscillation rate over the whole measurement period, denoted as $\hat{r}$, is defined as follows:

$$\hat{r} = \frac{1}{(t_n - t_1)} \int_{t_1}^{t_n} r(t)dt \tag{18}$$

where t_1 is the starting time of the measurement and t_n is the ending time of the measurement. We only have discrete phase samples. Suppose there are n samples in $\hat{\Theta}$. We approximately compute $\hat{r}$ as

$$\hat{r} = \frac{\sum_{\hat{\theta}(t) \in \hat{\Theta}} r(t) \times \Delta(t)}{\sum_{\hat{\theta}(t) \in \hat{\Theta}} \Delta(t)} \tag{19}$$

where $\Delta(t)$ is the time interval from sample $\hat{\theta}(t)$ to the next sample.

[1]Note that even though the phase curve is shown in our figures as a continuous line, it is in fact constructed by connecting the sequence of sampled phases.
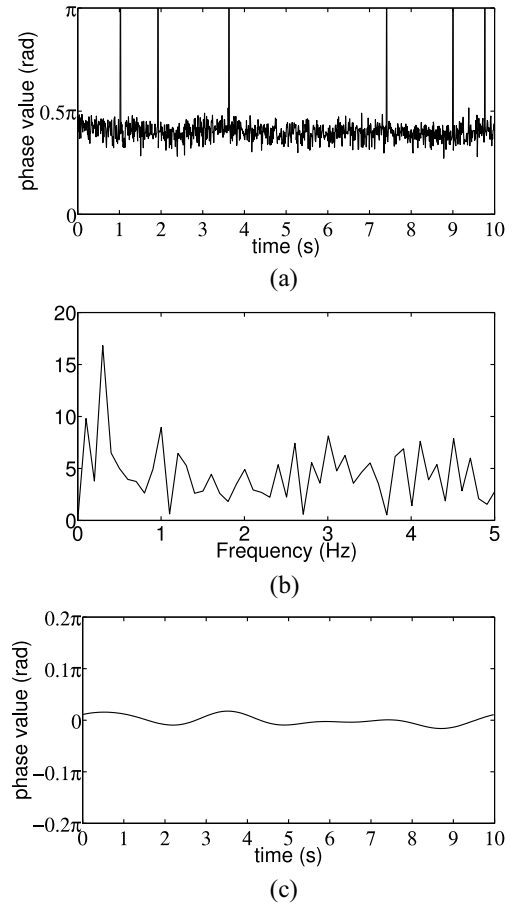

Fig. 7. Phase samples produced by a reader when a person breathes. (a) Phase samples when a person breathes. (b) Spectrum in frequency domain. (c) Phase samples after noise removal.

A similar procedure for period and rate estimations can be easily derived based on valleys.

F. Respiration Rate

Respiration rate is another important measurement of human health conditions. As mentioned earlier, the measurement scope of our system is not limited to hand tremor only. While the oscillation of human hands can be captured by the phase values of RFID tags, the oscillation of human chest, resulted from the action of breathing, can also be measured with the help of a tag. In this section, we leverage our system for estimating the respiration rate. To measure the respiration rate of a person, we attach a tag to the chest of the person. The reported phase values of the tag can reflect the person's chest movement, including the breathing rate. Again, the phase data suffers from noises caused by the RFID tags/reader and environment interference.

1) Respiration Rate of Static Person: We first measure the respiration rate of one static person. Fig. 7(a) shows the phase samples when a person breathes without any other bodily movement. The curve appears noisier than the tremor curve since the amplitude of breath is much smaller than hand tremor. We adopt similar data processing techniques as in Section IV-C to remove the noise. To extract the oscillation
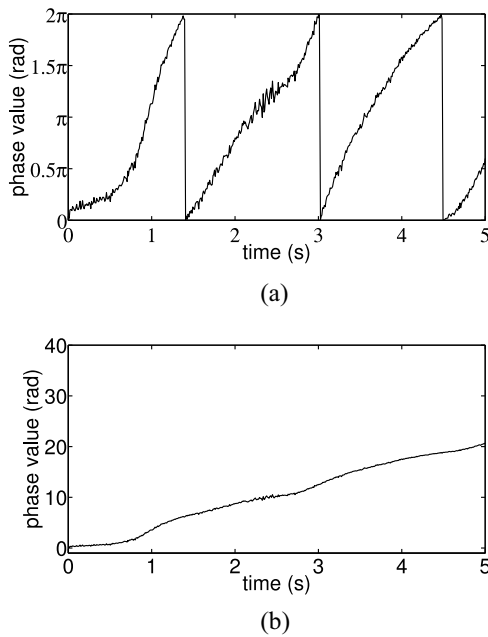
Fig. 8. Phase samples produced by a reader when a walking person breathes. Phase samples (a) when a walking person breathes and (b) after noise removal.

TABLE I
STANDARD DEVIATION OF PHASE SAMPLES AFTER NOISE/DC
REMOVAL UNDER DIFFERENT WALKING SPEEDS

walking speed (m/s)	std
0	0.13
0.1	3.27
0.3	8.49
0.5	13.15

observe that the measurement error will increase drastically as we further increase the moving speed beyond 0.1 m/s.

Although our system does not support respiration measurement in fast moving cases, it remains useful in practice. First, although 0.1-m/s movement is restrictive, it is still welcome because a patient does not have to be pinned to bed now, but instead can sit in a chair with normal body movements allowed, or even walk slowly. Second, as is explained above, an error of 1.56 b/min can be acceptable in health monitoring applications where deviation in respiration rate under abnormal conditions is expected to be much larger, for example, in short breath caused by heart or lung conditions. Third, we introduce a movement detection module for respiration measurement, which is able to detect the three cases below.

- *Case 1:* The patient is static. Our measurement is very accurate with a very small, negligible error.
- *Case 2:* The patient moves slowly (e.g., 0.1 m/s or lower). The average error is up to 1.56 b/min at 0.1 m/s measured from our experiments in Section VI.
- *Case 3:* The patient moves at a faster speed (e.g., higher than 0.1 m/s). The average error grows rapidly with the moving speed.

With the movement detection module, we know which case each measurement falls into. If the module indicates that a measurement is case 1, we know that it is accurate. If the module indicates that a measurement is case 2, we know that the error is much larger (up to 1.56 average) but still useable in certain applications. If it indicates that a measurement is case 3, we know that the error may be too large for the measurement to be used.

Given that movements such as walking can introduce a large variance into the oscillation signal as we can observe in Figs. 7(c) and 8(b), our movement detection module uses the standard deviation among the set of collected phase samples (after noise removal) to help determine which of the above three cases a person's movement belongs to. The idea is that the faster a patient moves, the more the noise will remain in the phase curve after noise/dc removal, which means a larger standard deviation. That is, indeed what we observe in our experiments as shown in Table I, where the measured standard deviation for case 1 is 0.13 when the patient does not move, that for case 2 is 3.27 when the patient moves at an average speed of 0.1 m/s, and it increases steadily for case 3 when the moving speed is beyond 0.1 m/s. Thanks to the large gap between these values, in our experimental evaluation (which will be reported in Section VI), we set two thresholds, 0.5 and 4, to empirically separate the three cases. If the standard deviation is smaller than 0.5, we classify it as case 1, which always results in very accurate rate measurement. If

pattern of human breathing, we perform extra analysis on the curve in frequency domain using fast Fourier transform (FFT). Fig. 7(b) shows the spectrum of the breathing curve in frequency domain and we can see there exists a frequency that dominates the phase curve. We then apply an FFT-based low pass filter to filter out high frequency components and apply an inverse FFT to the remaining coefficients to reconstruct the breathing signal. Fig. 7(c) shows the extracted breathing signal from the collected phase curve and a clear periodic pattern is extracted for period identification. Finally, we adopt the data processing techniques in Section IV-E for period identification. For multiperson cases, we attach a tag to each person, use the reported tag IDs to separate the phase values from different tags, and then process the phase values collected from each tag (person) separately to estimate the respiration rate of each person.

2) Respiration Rate of Moving Person: We then measure the respiration rate of a moving person. Fig. 8(a) shows the phase samples of breathing when a person walks at a speed of 0.1 m/s. Fig. 8(a) shows some periodic patterns, but they are caused by the module operation instead of respiration. Fig. 8(b) shows the phases samples after noise is removed. Compared to hand tremor, the oscillation introduced by respiration has smaller rate and magnitude, and its time-varying dc may dominate phase changes introduced by respiration, which can seriously degrade the measurement accuracy. For example, our experimental evaluation will show that the average measurement error is just 0.19 b/min for a static patient, while the average error becomes 1.56 b/min when the patient walks (has other bodily movement) at a low speed of 0.1 m/s, which is still useable, considering that the normal breathing rate is in the range of 12–24 b/min and that abnormal health conditions monitored based on respiration rate are likely to cause deviation far greater than 1.56 b/min from the normal. However, we
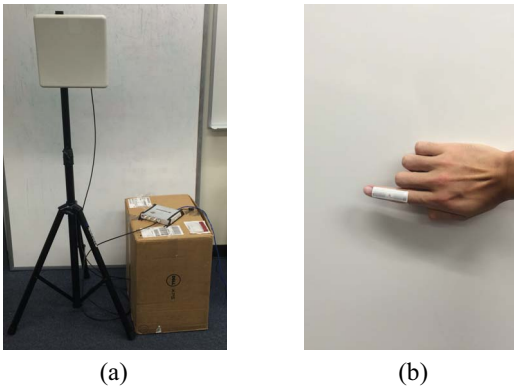
Fig. 9.   Experiment setup. (a) Reader and antenna. (b) RFID tag.

the standard deviation is between 0.5 and 4, we classify it as case 2, which results in an average error of up to 1.56 b/min in our experiments. If the standard deviation is larger than 4, we classify it as case 3. The actual thresholds in practice should be set based on application requirements. For example, if a monitoring application can tolerate an error of 5 b/min, one can certainly move up the threshold to allow more movement, which will be application-specific.

V. IMPLEMENTATION

We have implemented a prototype of our system as shown in Fig. 9. The system setup is given as follows.

A. RFID Reader

We use one commercial ImpinJ Speedway R420 reader [33] without any modifications on hardware or software. The reader is a Chinese version and operates in a fixed frequency within a range 920–925 MHz, as specified by the EPC C1G2 standard [37]. It provides four RP-TNC ports and thus can support up to four antennas. A GPIO Adapter [33] can be exploited to extend the number of connected antennas to 32, which significantly expands the coverage area of the reader. In our experiments, we set the reader in max throughput mode and use one Laird S9028PCLJ circular polarized antenna [40] as shown in Fig. 9(a), which is sufficient to cover our office area where the experiments are performed.

B. RFID Tags

We adopt widely used Alien Squiggle UHF RFID tags [41] whose dimensions are $1.752'' \times 0.409''$. They have an operation range up to 11 m. Those passive tags harvest energy from the RF signals emitted from the antenna. A tag is attached to the proper place on a human body to measure the oscillation rate of that part. Fig. 9(b) shows a tag attached to a finger.

C. Computer

We use a Dell XPS8500 desktop with Intel Core i7 CPU of 3.4 GHz to collect phase values from the reader and all collected data are processed in MATLAB.

VI. EVALUATION

We conduct experiments to evaluate the performance of our system. The experiments are carried out in an office with a dimension of 166×102 feet^2. The office environment contains furniture including desks, chairs, paper boxes, desktop and small appliances. We invite four volunteers to emulate hand tremor in our experiments. The volunteers tremble their hands at different rates in the range of 2–6 tps, which covers the typical tremor rate (4–6 tps) of a PD patient [42]. Each volunteer attaches one tag to one of his/her fingers for hand tremor rate measurement. Experiments are performed under different static/moving settings with a varying number of participants. Each experiment is repeated for 80 times to produce average results. The true oscillation rates are counted visually by recording the oscillation processing in videos. The estimated rates are compared with the true rates for error measurement. No previous health-monitoring systems are designed for measuring the hand tremor rate using RF signals.

To demonstrate that our system can be applied to other types of body oscillations, we use it to measure respiration rate by attaching a tag to the chest of each participant. We compare the performance of our system with UbiBreathe [6], CSI [34], and TagBreathe [18], which are designed for static setting where the participants do not move around.

A. Hand Tremor Rate Measurement

1) Hand Tremor Rate of One Static Person: Our first set of experiments use our system to measure the hand tremor rate of a single person who sits still in the office. The measurement results are given in Fig. 10.

Fig. 10(a) compares the measured tremor rate and the true tremor rate. Each point in the plot represents one experimental measurement, where the x coordinate is the true tremor rate and the y coordinate is the measured tremor rate. The equality line, $y = x$, is presented for reference: A point closer to the equality line is more accurate. We can see that most points are clustered around the equality line, demonstrating a good measurement accuracy of our system. Fig. 10(b) depicts the standard deviation of the measurement results when the hand tremor rate varies from 2 to 6 tps. All the points in Fig. 10(a) are placed in four bins, $[2, 3), \ldots, [5, 6]$. We compute the average bias in each bin, which is represented by the distance between the center bar in each bin and the equality line. The distance between the top (bottom) bar and the center bar is the standard deviation. Overall, the average measurement error our system is about 0.11 tps, which is accurate enough for most practical applications. Fig. 10(c) shows the cumulative density function (CDF) of the measurement error of hand tremor rate. For example, the 90 percentile of the measurement error is less than 0.3 tps. In conclusion, our system can yield very accurate measurement results of hand tremor rate for a single static person.

2) Hand Tremor Rate of One Moving Person: The second set of experiments use our system to measure the hand tremor rate when the person under monitoring is moving around in the office. We let our volunteer walk straight toward the antenna at a speed around 0.3 m/s with his hand trembling. Fig. 11(a)
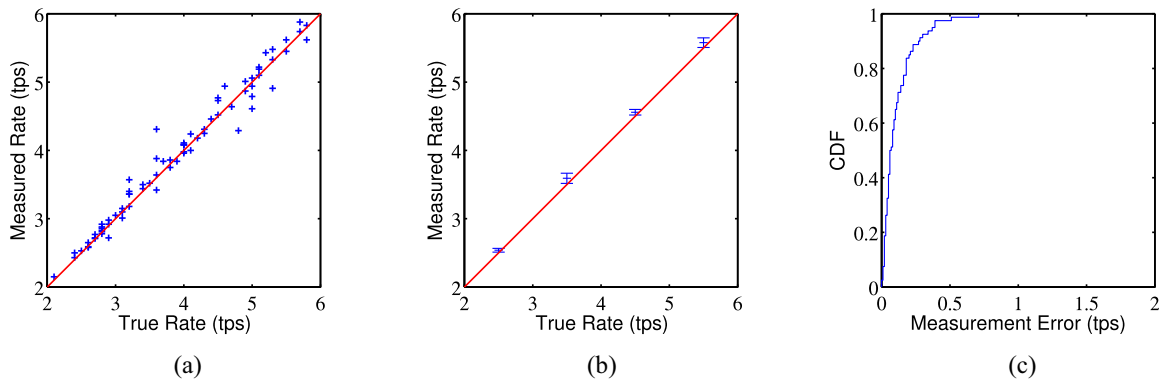
Fig. 10. Measurement accuracy of hand tremor rate of a single static person. (a) Measured oscillation rate. (b) Mean and standard deviation. (c) CDF of measurement error.
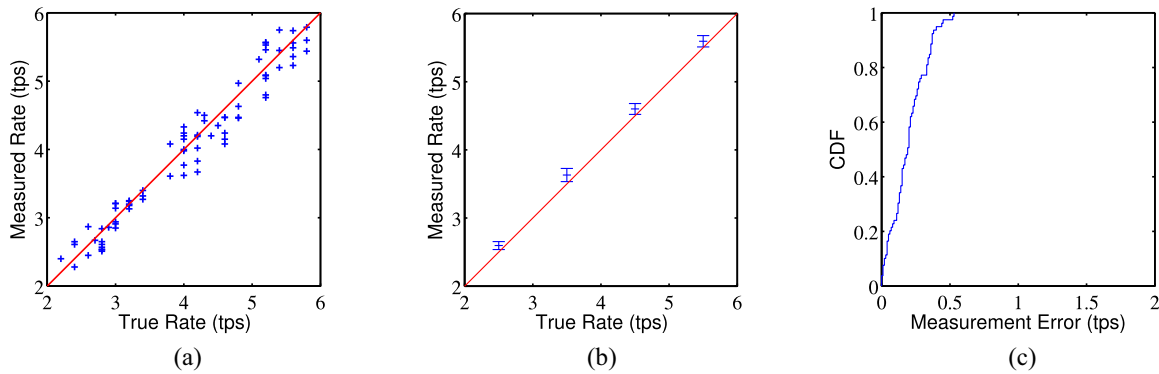

Fig. 11. Measurement accuracy of hand tremor rate of a single moving person. (a) Measured oscillation rate. (b) Mean and standard deviation. (c) CDF of measurement error.

presents the experimental results of measuring the hand tremor rate of a moving person. Again, most points cluster close to the equality line, demonstrating good performance. The measurement accuracy in terms of mean and standard deviation is presented in Fig. 11(b). The average measurement error is 0.21 tps, which is slightly larger than that of the static-person case in Section VI-A1. Besides, the CDF of the estimation error is presented in Fig. 11(c), where the 90 percentile of the error is less than 0.4 tps. These results demonstrate that the proposed system can accurately measure the hand tremor rate under the more challenging scenario where the person is moving.

3) Hand Tremor Rates of Multiple Static Persons: The third set of experiments use our system to measure the hand tremor rates of multiple static persons. We conduct experiments with 2, 3, and 4 volunteers, respectively, each with a tag attached to a finger.

Table II presents the mean errors and the standard deviations. In the second column, the mean measurement errors are 0.129, 0.127, and 0.142 tps for 2, 3, and 4 persons, respectively. It shows that the mean error is not very sensitive to the number of persons under monitoring. In the third column, the standard deviations are 0.103, 0.105, and 0.116, respectively; they are not very sensitive to the number of persons, either. The reason is that the collision-resolving arbitration protocol allows the reader to interrogate each tag individually and record its phase values based on its ID. Consequently, our system can

TABLE II
MEASUREMENT ACCURACY OF HAND TREMOR RATES (IN tps)
OF MULTIPLE STATIC PERSONS

number of people	average error	standard deviation
2	0.129	0.103
3	0.127	0.105
4	0.142	0.116

TABLE III
MEASUREMENT ACCURACY OF HAND TREMOR RATES (IN tps)
OF MULTIPLE MOVING PERSONS

number of people	average error	standard deviation
2	0.208	0.322
3	0.232	0.374
4	0.259	0.420

measure the oscillation rate on each tag without interference. Fig. 12 presents the CDF of the measurement error. For example, the 90 percentile of measurement error is less than 0.3 tps when four people are monitored simultaneously.

4) Hand Tremor Rates of Multiple Moving Persons: The fourth set of experiments evaluate the performance of our system for measuring hand tremor rates of 2, 3, or 4 moving persons simultaneously. We let our volunteers walk straight toward the antenna at a speed around 0.1 m/s. The results are shown in Table III, where the mean measurement errors are 0.208, 0.232, and 0.259 tps (in the second column) for 2, 3, and 4 persons, respectively. They are only slightly larger than
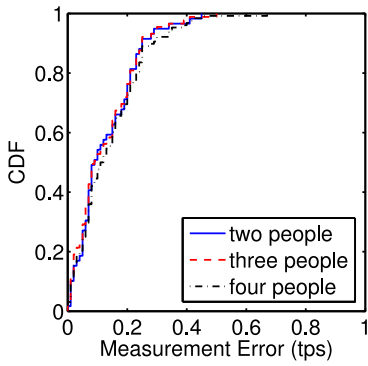
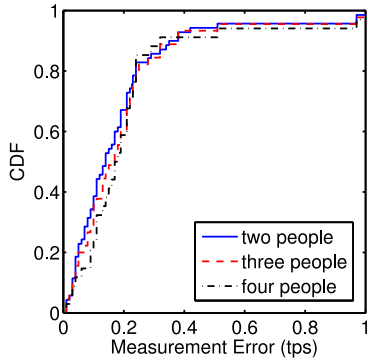Fig. 12. Error CDF for the measured hand-tremor rates of multiple static persons.

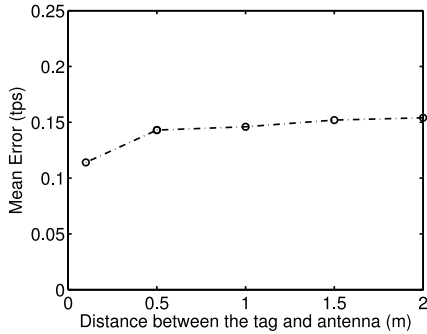Fig. 13. Error CDF for the measured hand-tremor rates of multiple moving persons.

Fig. 14. Mean error comparison on different distances between the tag and the antenna.

TABLE IV
MEASUREMENT ACCURACY OF HAND TREMOR RATES (IN tps)
WITH DIFFERENT WALKING SPEED

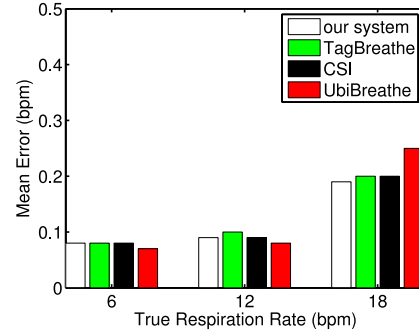| walking Speed (m/s)	average error	standard deviation
0.1	0.160	0.138
0.3	0.211	0.186
0.5	0.373	0.324

Fig. 15. Mean error comparison on the measured respiration rate of a single static person.

the lowest (0.114) when the distance is 0.1 m. As the distance increases, the mean measurement error slightly increases since the system will suffer more environmental interferences. But it still maintains a low level, smaller than 0.2 tps, which proves that our system can work scalably under different settings.

6) Impact of Walking Speed on One Person's Hand Tremor Rate: The sixth set of experiments use our system to evaluate the impact of the person's walking speed. In our experiments, we let the target person walk in a speed of 0.1, 0.3, and 0.5 m/s respectively, toward the antenna with his/her hand trembling.

Table IV presents mean errors and standard deviations of measuring a single person's hand tremor rate with different walking speed. The mean measurement error is the lowest (0.16) when the person walks slowly at a speed of 0.1 m/s. As the walking speed increases, the mean measurement error increases but still remains in an acceptable range. The increase of measurement error is expected since the performance of our time-varying dc removal algorithm degrades as the moving speed increases.

B. Respiration Rate Measurement

Finally, we evaluate the performance of our system in measuring another type of oscillation rate—chest oscillation rate caused by respiration. We compare the performance of our system with UbiBreathe [6], CSI [34], and TagBreathe [18], which are designed specifically for this task. Some of the prior works require restrictive settings and cannot measure multiple persons simultaneously.

1) One Static Person Scenario: We first measure the respiration rate of one person with a tag attached on his/her chest. The collected samples are also used to calculate ind and to test the false positive ratio of our movement detection module. Fig. 15 compares the measurement results of different systems when the person breaths at different rates. We observe that all four systems have comparable performance in measuring respiration rates. For example, when the person

the results in Table II for the static case. The standard deviations of the error are presented in the third column; they are all small. Fig. 13 shows the CDF of the measurement error. The 90 percentile of measurement error is about 0.4 tps when four people are monitored simultaneously.

5) Impact of Distance on One Static Person's Hand Tremor Rate: The fifth set of experiments use our system to evaluate the impact of distances between the tag and the reader's antenna. In our experiments, we let the target person sit still in the office trembling his hand and vary the distance between the hand(tag) and the antenna from 0.1 m to 2 m.

Fig. 14 presents mean errors of measuring a single person's hand tremor rate with different relative distances between the hand and the reader's antenna. The mean measurement error is

Fig. 16. Mean error comparison on the measured respiration rate of a single moving person.

Fig. 17. Mean error comparison on the respiration rates of two persons measured simultaneously.

breathes at a rate of 18 b/min, the mean measurement errors of our system, TagBreathe, CSI, and UbiBreathe are 0.19, 0.2, 0.2, and 0.25 b/min, respectively. Besides, the false positive ratio of our movement detection module is 0. As we can see, our system achieves a comparable performance with the other systems, which demonstrates that the design our system is generic in measuring bodily oscillations.

2) One Moving Person Scenario: We then measure the respiration rate of one moving person with a tag attached on his/her chest. We let our volunteer walk at a speed of around 0.1 m/s. Similarly, we also use the collected samples to test the false negative ratio of our movement detection module, with the two thresholds that separate the three moving cases as described in Section IV-F2 being 0.5 and 4. Recall that the detection module classify a measurement to be case 1 (static person) when the standard deviation in phase samples after noise/dc removal is less than 0.5, case 2 (slow movement at 0.1 m/s for example) when it is between 0.5 and 4, or case 3 (faster movement) when it is greater than 4. Fig. 16 shows the measurement CDF of our measurement result. The average measurement error is 1.56 b/min, which is eight times when compared with static scenarios and the false positive ratio of the movement detection module is 0. As we have explained earlier, although the error is much larger than that in static scenarios, we believe it is still useful in health-monitoring applications that can tolerate such an error, considering the normal breathing rate is much larger at 12–24 b/min. The benefit that comes with the error is the improved comfort that a patient can now enjoy, with no need to be pinned to a bed. When the moving speed is 0.2 m/s and higher, the errors in our experiments increase rapidly to be useable in practice.

3) Multiple Static Persons Scenario: The last set of experiments use our system to measure the respiration rates of multiple persons. Since UniBreathe and CSI are only able to concurrently measure up to two persons, we only evaluate the two-person case and the result is shown in Fig. 17, where the mean errors of these four systems are 0.29, 0.30, 0.4, and 0.41 b/min, respectively. All four systems still have comparable performance for measuring two persons' respiration rates, but the two RFID-based systems, our system and TagBreathe, perform better. This is benefitted from the design of commercial RFID systems, where tags can respond to the reader without interfering with each other's communication, which cannot be achieved by WiFi systems.
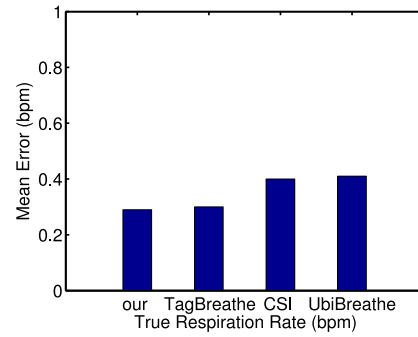
VII. Remarks and Limitations

In this section, we discuss some limitations of our system.

A. Walking

Our time-varying dc removal algorithm is designed to estimate and remove noise introduced for example by a patient's walking. When a patient walks at a speed less than 0.5 m/s (normal low-pace indoor walking which is expected from a PD patient who needs monitoring), our experimental evaluation has demonstrated good performance. In clinical settings, a patient, particularly an elderly PD patient, is more likely to move slowly, and our system can work well with hand tremor monitoring. However, when the person moves too fast relative to the monitored bodily oscillation, our noise removal method will not work well. This is evident in the measurement of respiration rate. Breathing generates very small chest movement, which translates into small magnitude in the measured phase curve. The typical rate of breathing (12–24 b/min) is much smaller than the typical tremor rate (4–6 tps), which means its phase curve has a much larger period. The combined effect is that respiration rate measurement is much more susceptible to the noise introduced by walking. Our experiments show that the proposed system can produce meaningful results only for slow walking scenarios, e.g., at a speed of 0.1 m/s, but the error will increase rapidly when the speed increases.

B. LOS

In general, RFID technology works with both LOS and non-LOS scenarios. However, our system tags human beings and cannot measure hand tremor in non-LOS scenarios, where RF signals are blocked by human bodies. The fluid in human body absorbs and reflects RF signals, preventing them from penetrating the body. The signals omitted by RFID antennas is not strong enough and the weak reflected RF signals in the environment do not offer reliable readings in our experiment.

VIII. Conclusion

In this paper, we design a novel wireless health-monitoring system using RFID tags. It provides a general and effective way of measuring oscillation rates. More specifically, the system uses the fine-grained phase values reported by an off-the-shelf RFID reader to estimate the oscillation rate

of a human body with great accuracy. The design supports the measurement of hand tremor rate of one person or the measurement of multiple persons simultaneously, even when the individuals move around, which represents a significant improvement over the previous systems. We have implemented a prototype and performed extensive experiments. Our experimental results demonstrate the effectiveness of our system in providing accurate rate measurements under challenging settings.

REFERENCES

[1] V. Shynayder, B.-R. Chen, K. Lorincz, T. R. F. F. Jones, and M. Welsh, "Sensor networks for medical care," in *Proc. ACM SenSys*, 2005, pp. 314–314.

[2] F. Adib, Z. Kabelac, H. Mao, D. Katabi, and R. C. Miller, "Demo: Real-time breath monitoring using wireless signals," in *Proc. ACM MobiCom*, 2014, pp. 261–262.

[3] N. Patwari, L. Brewer, Q. Tate, O. Kaltiokallio, and M. Bocca, "Breathfinding: A wireless network that monitors and locates breathing in a home," *IEEE J. Sel. Topics Signal Process.*, vol. 8, no. 1, pp. 30–42, Feb. 2014.

[4] J. Liu et al., "Tracking vital signs during sleep leveraging off-the-shelf WiFi," in *Proc. ACM MobiHoc*, 2015, pp. 267–276.

[5] F. Adib, H. Mao, Z. Kabelac, D. Katabi, and R. C. Miller, "Smart homes that monitor breathing and heart rate," in *Proc. ACM CHI*, 2015, pp. 837–846.

[6] H. Abdelnasser, K. A. Harras, and M. Youssef, "UbiBreathe: A ubiquitous non-invasive WiFi-based breathing estimator," in *Proc. ACM MobiHoc*, 2015, pp. 277–286.

[7] H. Wang et al., "Human respiration detection with commodity WiFi devices: Do user location and body orientation matter?" in *Proc. ACM UbiComp*, 2016, pp. 25–36.

[8] N. Lurie et al., "Preventive care: Do we practice what we preach?" *Amer. J. Public Health*, vol. 77, no. 7, pp. 801–804, 1987.

[9] J. T. Cohen, P. J. Neumann, and M. C. Weinstein, "Does preventive care save money? Health economics and the presidential candidates," *New England J. Med.*, vol. 358, no. 7, pp. 661–663, 2008.

[10] G. Joseph, N. J. Burke, N. Tuason, J. C. Barker, and R. J. Pasick, "Perceived susceptibility to illness and perceived benefits of preventive care: An exploration of behavioral theory constructs in a transcultural context," *Health Educ. Behav.*, vol. 36, pp. 71S–90S, Oct. 2009.

[11] M. M. Spencer-Smith et al., "Long-term benefits of home-based preventive care for preterm infants: A randomized trial," *Pediatrics*, vol. 130, no. 6, pp. 1094–1101, 2012.

[12] S. Patel et al., "Home monitoring of patients with Parkinson's disease via wearable technology and a Web-based application," in *Proc. IEEE EMBC*, 2010, pp. 4411–4414.

[13] *American Cancer Society Guidelines for the Early Detection of Cancer*. Accessed: Oct. 19, 2018. [Online]. Available: https://www.cancer.org

[14] S. Chakraborty, S. K. Ghosh, A. Jamthe, and D. P. Agrawal, "Detecting mobility for monitoring patients with Parkinson's disease at home using RSSI in a wireless sensor network," in *Proc. Int. Workshop Body Area Sensor Netw.*, 2013, pp. 956–961.

[15] C. A. Kushida et al., "Practice parameters for the indications for polysomnography and related procedures: An update for 2005," *Sleep*, vol. 28, no. 4, pp. 499–521, 2005.

[16] G. Albani et al., "Differences in the EMG pattern of leg muscle activation during locomotion in Parkinson's disease," *Funct. Neurol.*, vol. 18, no. 3, pp. 165–170, 2003.

[17] T. Hao, G. Xing, and G. Zhou, "iSleep: Unobtrusive sleep quality monitoring using smartphones," in *Proc. ACM Sensys*, 2013, p. 4.

[18] Y. Hou, Y. Wang, and Y. Zheng, "TagBreathe: Monitor breathing with commodity RFID systems," in *Proc. IEEE ICDCS*, 2017, pp. 404–413.

[19] A. Salarian et al., "Gait assessment in Parkinson's disease: Toward an ambulatory system for long-term monitoring," *IEEE Trans. Biomed. Eng.*, vol. 51, no. 8, pp. 1434–1443, Aug. 2004.

[20] D. Halperin, W. Hu, A. Sheth, and D. Wetherall, "Tool release: Gathering 802.11n traces with channel state information," *ACM SIGCOMM Comput. Commun. Rev.*, vol. 41, no. 1, p. 53, 2011.

[21] L. Yang, Y. Li, Q. Lin, X.-Y. Li, and Y. Liu, "Making sense of mechanical vibration period with sub-millisecond accuracy using backscatter signals," in *Proc. ACM MobiCom*, 2016, pp. 16–28.

[22] *Kinesia 360*. Accessed: Oct. 19, 2018. [Online]. Available: http://glneurotech.com/kinesia/

[23] A. T. Tzallas et al., "PERFORM: A system for monitoring, assessment and management of patients with Parkinson's disease," *Sensors*, vol. 14, no. 11, pp. 21329–21357, 2014.

[24] T. Li, S. Chen, and Y. Ling, "Identifying the missing tags in a large RFID system," in *Proc. ACM MobiHoc*, Sep. 2010, pp. 1–10.

[25] L. Yang et al., "Tagoram: Real-time tracking of mobile RFID tags to high precision using COTS devices," in *Proc. ACM MobiCom*, 2014, pp. 237–248.

[26] J. Wang, F. Adib, R. Knepper, D. Katabi, and D. Rus, "RF-compass: Robot object manipulation using RFIDs," in *Proc. ACM MobiCom*, 2013, pp. 3–14.

[27] L. Xie, H. Han, Q. Li, J. Wu, and S. Lu, "Efficiently collecting histograms over RFID tags," in *Proc. IEEE INFOCOM*, 2014, pp. 145–153.

[28] M. Chen, W. Luo, Z. Mo, S. Chen, and Y. Fang, "An efficient tag search protocol in large-scale RFID systems," in *Proc. IEEE INFOCOM*, Apr. 2013, pp. 899–907.

[29] L. Yang, Q. Lin, X. Li, T. Liu, and Y. Liu, "See through walls with COTS RFID system," in *Proc. ACM MobiCom*, 2015, pp. 487–499.

[30] J. Liu, Y. Zhang, M. Chen, S. Chen, and L. Chen, "Collision-resistant communication model for stateless networked tags, poster paper," in *Proc. IEEE ICNP*, 2016, pp. 64–65.

[31] Y. Zhang, S. Chen, Y. Zhou, and Y. Fang, "Anonymous temporal-spatial joint estimation at category level over multiple tag sets," in *Proc. IEEE INFOCOM*, 2018, pp. 846–854.

[32] Y. Zhang, S. Chen, Y. Zhou, and O. Odegbile, "Missing-tag detection with presence of unknown tags," in *Proc. IEEE SECON*, 2018, pp. 1–9.

[33] *ImpinJ*. Accessed: Oct. 19, 2018. [Online]. Available: http://www.impinj.com/

[34] T. Ballal, R. B. Shouldice, C. Heneghan, and A. Zhu, "Tracking vital signs during sleep leveraging off-the-shelf WiFi," in *Proc. IEEE BioWireless*, 2012, pp. 267–276.

[35] Y. Chen and P. Rapajic, "Human respiration rate estimation using ultra-wideband distributed cognitive radar system," *Int. J. Autom. Comput.*, vol. 5, no. 4, pp. 325–333, 2008.

[36] A. Lazaro, D. Girbau, and R. Villarino, "Analysis of vital signs monitoring using an IR-UWB radar," *Progr. Electromagn. Res.*, vol. 100, pp. 265–284, 2010. [Online]. Available: http://www.jpier.org/PIER/pier.php?paper=09120302

[37] *EPC Radio-Frequency Identity Protocols Class-1 Gen-2 UHF RFID Protocol for Communications at 860MHz-960MHz, EPC Global*. Accessed: Oct. 19, 2018. [Online]. Available: http://www.epcglobalinc.org/uhfclg2

[38] M. Wachowiak, G. Rash, P. Quesada, and A. Desoky, *Comparison of Wavelet-Based and Traditional Noise Removal Techniques*, Gait Biomech. Lab., Univ. Louisville, Louisville, KY, USA, Aug. 1998.

[39] D. L. Donoho and I. M. Johnstone, *Ideal Spatial Adaptation by Wavelet Shrinkage*, Dept. Stat., Stanford Univ., Stanford, CA, USA, Apr. 1993.

[40] *Laird*. Accessed: Oct. 19, 2018. [Online]. Available: http://www.lairdtech.com/products/s9028PCL

[41] *AlienTags*. Accessed: Oct. 19, 2018. [Online]. Available: http://www.alientechnology.com/products/tags/squiggle/

[42] M. Mario et al., "Bioinformatic approaches used in modelling human tremor," *Current Bioinformat.*, vol. 4, no. 2, pp. 154–172, 2009.

Youlin Zhang (GS'17–M'18) received the B.S. degree in electronic information engineering from the University of Science and Technology of China, Hefei, China, in 2014. He is currently pursuing the Ph.D. degree in computer and information science and engineering at the University of Florida, Gainesville, FL, USA, under the supervision of Prof. S. Chen.
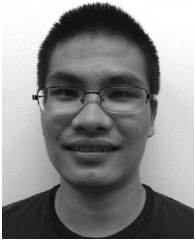
His current research interests include big network data and Internet of Things.

Shigang Chen (A'03–M'04–SM'12–F'16) received the B.S. degree in computer science from the University of Science and Technology of China, Hefei, China, in 1993, and the M.S. and Ph.D. degrees in computer science from the University of Illinois at Urbana–Champaign, Urbana, IL, USA, in 1996 and 1999, respectively.
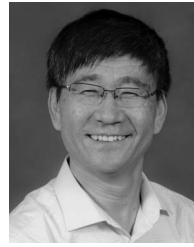
He is a Professor with the Department of Computer and Information Science and Engineering, University of Florida, Gainesville, FL, USA. He was with Cisco Systems, San Jose, CA, USA, for three years before joining the University of Florida, in 2002. He has been holding the University of Florida Research Foundation Professorship and the University of Florida Term Professorship since 2017. He has authored or co-authored over 190 peer-reviewed journal/conference papers. He holds 12 U.S. patents. His current research interests include computer networks, big data, Internet security, RFID, cyber-physical systems, and wireless communications.

Dr. Chen was a recipient of the IEEE Communications Society Best Tutorial Paper Award and the NSF CAREER Award. He is an Associate Editor of the IEEE TRANSACTIONS ON MOBILE COMPUTING, and served on the Editorial Board for the IEEE/ACM TRANSACTIONS ON NETWORKING, the IEEE TRANSACTIONS ON VEHICULAR TECHNOLOGY, the *Journal of Computer Networks* (Elsevier), and *ZTE Communications*. He served in various Chair positions or as a Technical Committee member for numerous conferences. He is an ACM Distinguished Member.

Yuguang Fang (S'92–M'93–SM'99–F'08) received the Ph.D. degree in systems engineering from Case Western Reserve University, Cleveland, OH, USA, in 1994, and the Ph.D degree in electrical engineering from Boston University, Boston, MA, USA, in 1997.

He was an Assistant Professor with the Department of Electrical and Computer Engineering, New Jersey Institute of Technology, Newark, NJ, USA, from 1998 to 2000. He then joined the Department of Electrical and Computer Engineering, University of Florida, Gainesville, FL, USA, in 2000, as an Assistant Professor, and became an Associate Professor with tenure in 2003 and a Full Professor in 2005. He held the University of Florida Research Foundation Professorship from 2006 to 2009, a Changjiang Scholar Chair Professorship with Xidian University, Xi'an, China, from 2008 to 2011, and a Guest Chair Professorship with Tsinghua University, Beijing, China, from 2009 to 2012. He has authored or co-authored over 250 papers in refereed professional journals and conferences.

Dr. Fang was a recipient of the National Science Foundation Faculty Early Career Award in 2001, the Office of Naval Research Young Investigator Award in 2002, the Best Paper Award of the IEEE International Conference on Network Protocols in 2006, and the IEEE TCGN Best Paper Award of the IEEE High-Speed Networks Symposium and IEEE GLOBECOM, in 2002. He is also active in professional activities. He is currently serving as the Editor-in-Chief for *IEEE Wireless Communications* and serves/served on several Editorial Boards of technical journals. He is a member of the ACM.

You Zhou (GS'16–M'17) received the B.S. degree in electronic information engineering from the University of Science and Technology of China, Hefei, China, in 2013. He is currently pursuing the Ph.D. degree in computer and information science and engineering at the University of Florida, Gainesville, FL, USA, under the supervision of Prof. S. Chen.

His current research interests include network security and privacy, big network data, and Internet of Things.

Chen Qian (S'08–A'08–M'13) received the B.S. degree in computer science from Nanjing University, Nanjing, China, in 2006, the M.Phil. degree in computer science from the Hong Kong University of Science and Technology, Hong Kong, in 2008, and the Ph.D. degree in computer science from The University of Texas at Austin, Austin, TX, USA, in 2013.

He is currently an Assistant Professor with the Department of Computer Engineering, University of California at Santa Cruz, Santa Cruz, CA, USA. He has authored or co-authored over 60 research papers in highly competitive conferences and journals. His current research interests include computer networking, network security, and Internet of Things.